BIW10 Preprint -- Edited; preliminary green dot status
Final version will appear on JACoW

MODELING THE OPTICAL COUPLING EFFICIENCY OF THE LINAC COHERENT LIGHT SOURCE BEAM LOSS MONITOR RADIATOR*

J. C. Dooling, W. Berg, and B.X. Yang, ANL, Argonne, IL 60439, USA
M. Santana Leitner, A. S. Fisher, and H.-D. Nuhn, SLAC NAL, Menlo Park, CA 94025, USA

Abstract

A large-solid-angle, Cherenkov detector beam loss monitor has been built and tested as part of the Linac Coherent Light Source machine protection system (MPS). The MPS is used to protect the undulator magnets by detecting high-energy electron beam loss. These electrons produce other forms of radiation that can lead to demagnetization of the undulator magnets. Cherenkov light is generated when primary electrons, lost from the beam, create a shower of secondary electrons that transit through the Cherenkov radiator medium. The radiator consists of an Al-coated plate of high-purity, fused-silica 12.77 cm wide, 6.29 cm high, and 0.64 cm thick, which is formed into a tuning fork geometry that envelopes the beam pipe preceding each undulator. The radiator transports Cherenkov photons via internal reflection through a tapered region and stem into the photocathode of a compact photomultiplier tube (PMT).

We calculate the optical efficiency of the radiator η_c, that is, the probability that a photon generated within the fused silica will reach the exit aperture adjacent to the PMT. A simple model based on line sources summed across image planes is compared for the case of normally incident electrons with a more detailed Monte Carlo random-walk simulation called RIBO[1]. Both analytical and numerical models show the efficiency to be relatively uniform over the full range of transverse locations in the radiator. This is encouraging for the MPS detection scheme, which seeks to protect the undulator magnets over their entire cross section. As we expect, both analyses show η_c to be a strong function of the surface reflectivity R_f; η_c ~0.0084 for R_f=0.95, but drops to 0.0033 for R_f=0.90.

INTRODUCTION

High-energy electrons lost from third- or fourth-generation light source beams can lead to the generation of star events, which are strongly correlated with the demagnetization of undulator magnets[2]. Cherenkov radiation provides a natural method to observe beam loss from these machines[3]. Cherenkov radiators fabricated from high-purity, fused-silica have several desirable characteristics for detection of high-energy electrons. First, they can withstand high levels of radiation without darkening or suffering degraded transmission[4]; second, they offer immunity to scintillation noise from lower-energy x-ray photons; third, Cherenkov radiation is produced at optical wavelengths that can be detected with high-gain photomultiplier tubes (PMTs) providing low electrical noise signals.

The Linac Coherent Light Source (LCLS) beam loss monitor (BLM) diagnostic for the free-electron laser (FEL) undulators is composed of a fused-silica radiator encased in an anodized aluminum housing. The BLM is part of the LCLS machine protection system; as such, the radiator seeks to cover a broad area of transverse space or large solid angle to fully monitor beam loss into the FEL magnets. The radiator is roughly in the shape of a “tuning fork” or “Y” where the re-entrant cutout of the fork is occupied by the electron beam vacuum vessel. The BLM is integrated with the beam finder wire diagnostic located just upstream of each undulator magnet. A cross section of the BLM is presented in Figure 1. The large parallel surfaces (z-planes) of the radiator are polished to optical grade flatness; whereas, the x- and y-planes edge surfaces are flame polished. The entire radiator is coated with a reflective layer of aluminum; the exceptions being the exit aperture facing the PMT detector and two small circular areas in the stem, one of which is used to introduce a ``heartbeat" optical pulse.

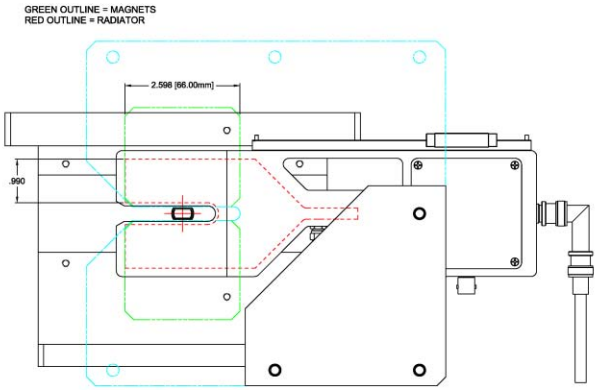

Figure 1: Cross sectional view of the beam loss monitor; view is looking upstream.

MODELING

The generation of photons from a super-luminal electron traversing a transparent medium of index of refraction n_r has been discussed in detail by a number of authors, for example[5,6].

*Work supported by the U.S. D.O.E. Office of Science, Office of Basic Energy Sciences, under contract numbers DE-AC02-06CH11357 and DE-AC02-76SF00515.

#dooling@aps.anl.gov

Analytic Image Line Source Approximation

A simple model based on normally incidence electrons is presented. We assume all electrons are energetic enough to completely traverse the radiator and remain above the minimum energy for Cherenkov light production; therefore, the path-length must exceed 0.64 cm, and the minimum energy may be determined from the Frank-Tamm formula[7],

$$dE=\frac{\mu(\omega)}{4\pi}e^2\omega\left[1-\frac{1}{n_r^2(\omega)\beta^2}\right]dx\,d\omega\,, \tag{1}$$

where ω is the angular frequency and μ(ω) and $n_r(\omega)$ are frequency-dependent permeability and index of refraction of the medium. The number of photons generated per electron over an incremental path length dx and frequency dω may be expressed as,

$$dN_p=\frac{dE}{\hbar\omega}=\frac{\alpha}{c}\mu_r(\omega)\left[1-\frac{1}{n_r^2(\omega)\beta^2}\right]dx\,d\omega\,, \tag{2}$$

where the fine structure constant $\alpha=e^2c\mu_o/2h$. We assume the material is non-magnetic at optical frequencies, therefore $\mu(\omega)=\mu_o$. Integrating over frequency, we obtain,

$$\frac{dN_p}{dx}=N_o(\omega_2,\omega_1)\left[1-\frac{1}{n_r^2\beta^2}\right], \tag{3}$$

where n_r represents the average refractive index over the frequency range and

$$N_o(\omega_2,\omega_1)=\frac{\alpha}{c}(\omega_2-\omega_1). \tag{4}$$

For ω in the optical range of frequencies defined by λ_1=600 nm and λ_2=150 nm,

$$N_o=2.35\text{x}10^3\,\frac{photons}{cm}. \tag{5}$$

The minimum energy for generation of Cherenkov radiation in the fused-silica radiator occurs when $v/c=\beta \geq n_r^{-1}$. At 400 nm, for example, n_r=1.47 and β_{min}=0.680, corresponding to a kinetic energy of 0.186 MeV. At this energy, the range of an electron in the radiator is short. The range may be expressed as,

$$t_r^{-1}=-\left[\frac{1}{\rho}\frac{dE}{dx}\right]\frac{\rho_{SiO_2}}{E}. \tag{6}$$

According to CSDA data for SiO_2[8], the mass stopping power in fused silica for a 0.2-MeV electron is 2.323 MeV-cm^2-g^{-1}; therefore, t_r=0.037 cm (ρ_{SiO2} =2.32 g/cm^3). The number of Cherenkov photons depends on the total path length and on electron kinetic energy as ln(kγ), where k is a constant. Thus, the number of photons initially grows rapidly with energy then effectively saturates as the path length exceeds the thickness of the radiator, d_r. The electron range exceeds the radiator thickness at kinetic energies of 2.4 MeV and above. For high-energy electrons (>4 MeV, β≈1), the index defines the opening angle of the Cherenkov cone, $\theta_c=\cos^{-1}(n_r^{-1})$ =47.1°.

The number of photons reaching the exit aperture from an incident electron located at a distance r_i may be expressed as,

$$N_{ap}=\sum_i^N S(r_i)\,T_{r_i}\,\delta A\,, \tag{7}$$

where δA is the area of the radiator exit aperture ($\delta A=d_r^2$) and $r_i=(x_i^2+y_i^2)^{1/2}$. The line source intensity is given by,

$$S(r_i)=\frac{N_o}{2\pi r_i}, \tag{8}$$

and the transmission function incorporating multiple reflections from the coated surface can be written as,

$$T_{r_i}=R_f^{n_{bi}}, \tag{9}$$

where R_f is the reflection coefficient of the aluminum coating, and n_{bi} is the number of bounces from the i^{th} source or image. All image locations are determined in terms of the source position. The distance travelled by the photons from the electron source to the exit aperture will be lengthened by $\sec(\theta_c)=\beta n_r$. The actual distance travelled by the photons from one radiator face to another is the length of the hypotenuse, $l_h=d_r\sec(\theta_c)$ as shown in Figure 2. The horizontal distance covered in one bounce is $l_b=l_h\sin(\theta_c)=d_r\tan(\theta_c)$; if the line-of-sight distance from the source (or image) to the exit face is R_s, then the number of bounces can be calculated as $n_b=R_s/l_b$. The total distance a photon must travel from source to exit face is then $R_T=n_b l_h$. We then define the coupling efficiency as $\eta_c=N_{ap}/(N_o d_r)$.

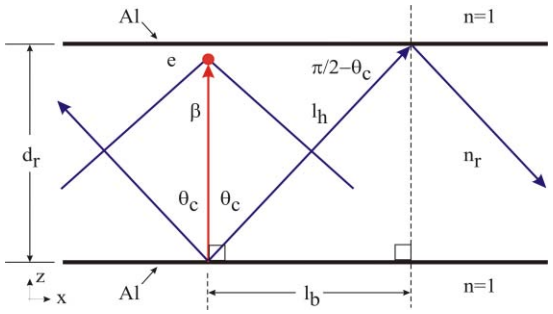

Figure 2: Radiator geometry with normally incident electron.

Looking at just the fork volume closest to the beam, the y-averaged coupling efficiency profile, η_{cx} is determined from the incident electron position and three additional image locations as indicated in Figure 3. Horizontal distance is measured from the radiator exit aperture. The y-averaged coupling efficiency η_{cx} is calculated for possible coating reflectivities of 0.85, 0.90, and 0.95 and plotted versus distance to the radiator aperture in Figure 4. Ideally, we want the response of the radiator to be as uniform as possible over the x-y region shared by the undulator magnets. Figure 5 presents the y-averaged η_{cx} assuming a 3-image model normalized by the average coupling efficiency over the range of x, $\langle\eta_{cx}\rangle$; that is, $\rho=\eta_{cx}/\langle\eta_{cx}\rangle$. Uniformity is seen to improve with higher coating reflectivities. The mean coupling efficiency values in the tuning fork regions seen in Figs. 4 and 5 are presented in Table 1. The distribution of coupling

efficiency predicted by the image model is presented in Figure 6.

Table 1: Mean Radiator η_c in the Tuning Fork

R_f	η_c
0.95	8.4×10^{-3}
0.9	3.3×10^{-3}
0.85	1.4×10^{-3}

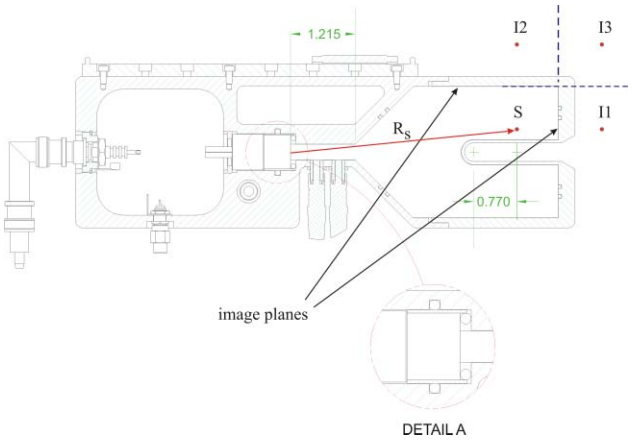

Figure 3: Incident electron position (S) and 3 image locations (I1-I3) in the BLM radiator. View is looking downstream.

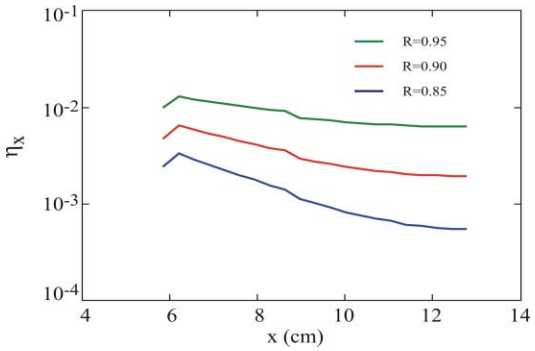

Figure 4: Y-averaged η vs. horizontal distance from the radiator exit aperture for R_f=0.85, 0.90, and 0.95.

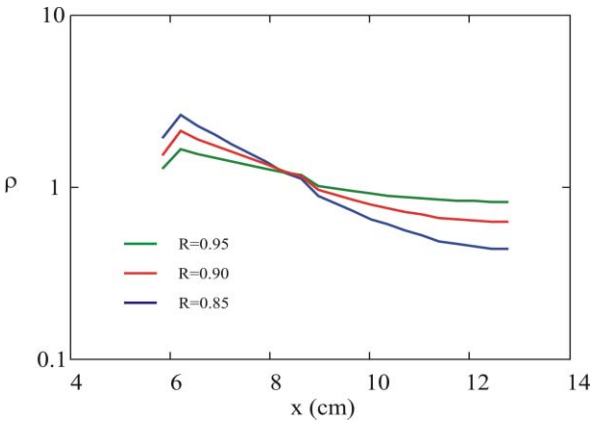

Figure 5: Ratio of y-averaged η normalized to its own mean value vs. horizontal distance from the radiator exit aperture for R_f=0.85, 0.90, and 0.95.

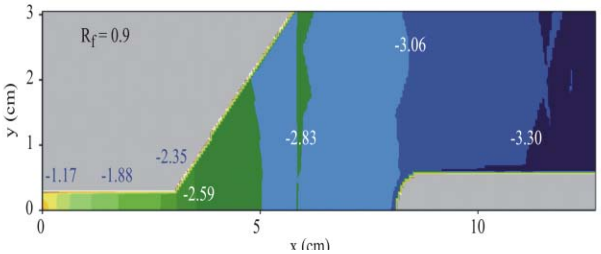

Figure 6: Coupling efficiency distribution in the radiator predicted by the image model for R_f=0.9 ($\log_{10}$ scale).

Monte Carlo Simulation of the Optical Coupling using the RIBO Code

Not only did the previous analytic model advance which coupling efficiencies can be expected from these BLMs, but also it will be instrumental to validate the applicability of the random-walk RIBO[1] simulation code, typically used for low-energy ion-transport problems but also capable to track photons. In future studies, this 3D Monte Carlo program will be used in conjunction with intranuclear cascade codes (i.e., FLUKA, MARS15[9]) to estimate the signals in the LCLS BLMs from showers generated and propagated along the radiation-sensitive undulator.

For this first-order study of the optical coupling of LCLS BLMs, electrons were assumed to hit perpendicularly against the front face of the quartz. This scenario represents the higher energy electrons, which are those with greater Cherenkov yield (N_p), as shown in Eq. 2. Photons were generated with uniform azimuthal angle at θ_c=47° from the normal. The birth coordinates of the photons were sampled within the full BLM so as to study the optical coupling as a function of the electron impact position at any point.

In this model, photons moved in straight paths between any two consecutive (elastic) collisions with the aluminum coating. The RIBO printing function was customized to dump, for every photon, its initial coordinates, the number of collisions with the coating walls from birth till collection in the photocathode, and the corresponding flight path through the quartz. With these data, for a given reflection coefficient, the "intensity" of any out-coming photon can be computed by using Eq. 9. Moreover, for detailed calculations with real showers, the individual flight path could be used to compute the attenuation of photons through the radiator material, although this factor is mostly negligible in quartz for Cherenkov light.

Computations were parallelized in the SLAC UNIX farm, where they ran as fast as 100 histories/s-CPU. Individual events were post-processed to sort them into 3.2 x 2.0 mm² pixels. The resulting efficiency maps were formatted like FLUKA[10, 11] USRBIN files, so that the FLAIR[12] GNUPLOT interface could be used to plot the data. Those are shown in Figure 7a-c for three reflection coefficients, R_f=0.95, 0.90 and 0.85, respectively. Fig. 7d

shows the R_f=0.90 case when the Cherenkov angle is 9% larger.

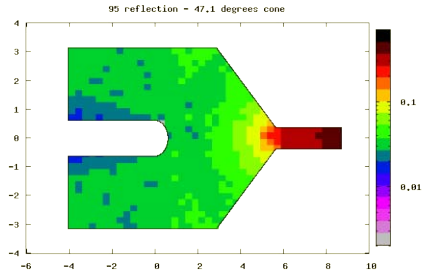

Figure 7a: θ_c=47.1°, R_f=0.95.

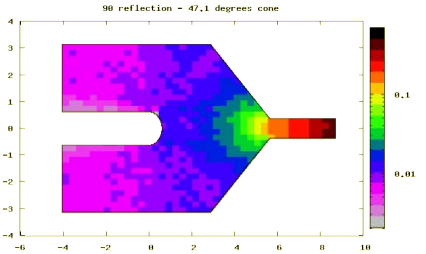

Figure 7b: θ_c=47.1°, R_f=0.90.

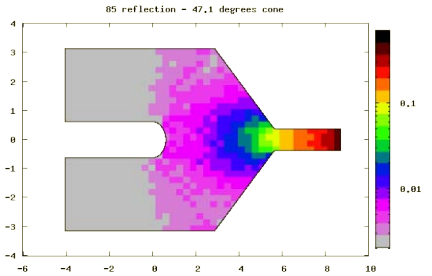

Figure 7c: θ_c=47.1°, R_f=0.85.

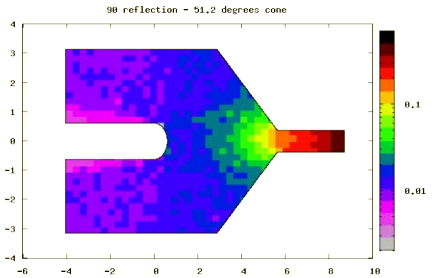

Figure 7d: θ_c=51.2°, R_f=0.90.

We observe consistency between the Monte Carlo results of Fig. 7 and the analytical curves of Fig. 4. This will allow performing more complex studies (i.e., BLM geometry optimization, realistic beam loss transport) with confidence in RIBO simulation results.

BEAM LOSS MEASUREMENT AND SIMULATION

Initially, five BLMs have been installed in the LCLS, on girders 1, 9, 17, 25, and 33; the full complement of 33 BLMs, one for each girder, will be installed this summer. During restart of the facility in April, a set of loss measurements were conducted with the beam finder wire (BFW) system. The BFW tests are used to verify BLM operation and obtain indications of beam position offsets and size in both horizontal (x) and vertical (y) planes. The LCLS undulator region has been modeled with the Monte-Carlo particle tracking codes MARS[13] and FLUKA to facilitate calibration of the BLMs. Beam loss electron fluence in the radiators is examined simultaneously with radiation deposition in the undulator magnets. For computational efficiency, we run the LCLS MARS model assuming a single loss point (for example, BFW01) and score electron fluences in all 33 radiators along the 132-m length of the undulator section. The BFW survey on the other hand, will use multiple loss points and then monitor the signal at a fixed BLM location, such as girder 33. Aside from the undulators, beam optics in the FEL section is that of a simple FODO lattice, which, with proper matching upstream, provides beam envelopes with modest betatron oscillations in both planes. Quadrupole focusing in the FEL is included in the Monte Carlo models. Because of the regularity in the beam in the FEL, we can compare the single point loss, multiple detector simulations with the multiple position loss, single detector profile by flipping the direction of the z-axis in the simulation case and then overlaying the result on the BFW/BLM measurements. This allows us a rough idea of how well the measurement and simulation agree. A comparison of measurement and simulation results using this method is presented in Figure 8. In the simulation, an average coupling efficiency of 1.4×10^{-3} is employed representing a reflectivity of 85%. We note that BFW data is not present from girders 9, 10, 11, 32, and 33 in x and girders 1, 8, 23, and 33 in y. Missing data in the simulation represents radiators that scored no events. The main burst of electron fluence occurs within the first 14 girders of the loss point; this is seen in both measurement and simulation.

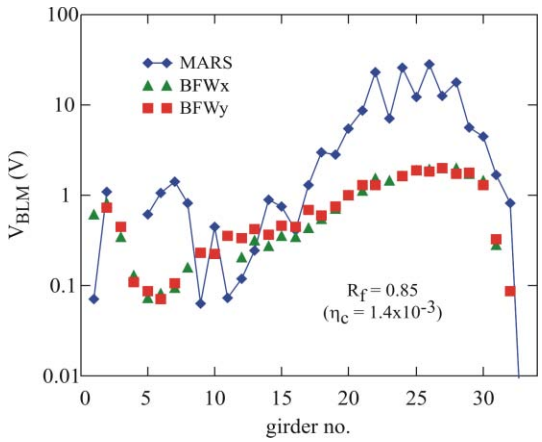

Figure 8: Comparison of BFW BLM loss measurements (single detector, multiple loss points) with MARS (multiple detectors, single loss point at BFW01).

DISCUSSION AND CONCLUSION

The curved surface of the cut-out acts as a defocusing cylindrical mirror; this and the wedge make the geometry difficult to model realistically with line sources. Note that the radiator region in the fork, closest to the vacuum chamber, is blocked from direct view of the exit aperture by the cut-out. This effect is seen in both models. In the line image model, conditions on the images are applied depending on the source position in x. In the simplified line-image model, effects such as diffraction around edges have been ignored.

The rapid reduction in coupling efficiency with distance from the exit aperture has been qualitatively verified by measurements carried out on a BLM prototype at the ANL Advanced Photon Source (APS)[14]. In reality, not all electrons will be entering the radiator at normal incidence; therefore, the single-angle bounce model is insufficient, and numerical approximations must be used. Finally, the Cherenkov cone angle of photon propagation is the same as the condition for total internal reflection; therefore steps must be taken to prevent large reflection at the exit face aperture. These steps can include using optical grease or introducing a wedge at the output aperture.

Regarding comparison of measurement and simulation, we see a relatively poor agreement in the prediction of signal intensity; in order to match the peak predicted signals with measurements, $\eta \leq 2.4x10^{-4}$ is required, corresponding to a reflectivity of 75%. We believe this is too low and must look elsewhere for the discrepancy. For example, maximum output voltages from the BLM electronics might be exceeded in the high-radiation regions leading to saturation.

Though the simple, line-image model presented here is insufficient to accurately predict the coupling coefficient, it does provide a method to address important radiator characteristics, such as coupling uniformity. More precise Monte Carlo methods, such as RIBO, are necessary to examine the effect of arbitrary electron incidence angles and energies.

REFERENCES

1. M. Santana Leitner, *A Monte Carlo code to optimize the production of radioactive ion beams by the ISOL Technique*, Ph.D. Thesis, UPC-ETSEIB (2005), CERN-THESIS-2006-031, 311 p.
2. Y. Asano, T. Bizen, and X. Marechal, J. Synchrotron Rad. **16** (2009), 317-324.
3. G.F. Knoll, *Radiation Detection and Measurement*, Wiley, New York, 1989, p. 682.
4. J. Cohen-Tanugi, et al., Nuc. Instrum. Meth. A **515** (2003), 680-700.
5. J.V. Jelley, British Journal of Applied Physics, **6** (1955), 227-232.
6. J.D. Jackson, *Classical Electrodynamics*, Wiley, New York, 1975, p. 638.
7. I.E. Tamm and I.M. Frank, Dokl. Akad. Nauk USSR **14** (1937) 109.
8. International Commission on Radiation Units and Measurements. ICRU Report 37, *Stopping Powers for Electrons and Positrons*.
9. N. Mokhov and S. Striganov, "MARS 15 overview," Tech. Report Fermilab-Conf-07/008-AD, 2007.
10. G. Battistoni, S. Muraro, P.R. Sala, F. Cerutti, A. Ferrari, S. Roesler, A. Fasso, *The FLUKA code: Description and benchmarking*, Proceedings of the Hadronic Shower Simulation Workshop 2006, Fermilab 6-8 September 2006, M. Albrow, R. Raja, eds., AIP Conference Proceeding 896, 31-49, (2007).
11. A. Fasso, A. Ferrari, J. Ranft and P.R. Sala, CERN-2005-10 (2005), INFN/TC_05/11, SLAC-R-773.
12. V. Vlachoudis, *FLAIR: A Powerful But User Friendly Graphical Interface For FLUKA*, Proc. Int. Conf. on Mathematics, Computational Methods & Reactor Physics, (M and C 2009), Saratoga Springs, New York, 2009.
13. W. Berg et al., Proceedings of LINAC08, Victoria, BC, Canada, (2008) 493-494.
14. B.X. Yang, et al., these proceedings.